Vertically polarized lasing and photoluminescence in a ridge quantum-wire laser

Shinichi Watanabe,* Shyun Koshiba,† MasahiroYoshita, Motoyoshi Baba, Hiroyuki Sakaki,‡ and Hidefumi Akiyama
Institute for Solid State Physics, University of Tokyo, 5-1-5, Kashiwanoha, Kashiwa, Chiba, 277-8581, Japan
(Received 2 February 2003; published 18 November 2003)

We study vertically polarized lasing and spontaneous emissions in a ridge quantum-wire (QWR) laser. In particular, we find that most of emissions with energies near the band edge are vertically polarized. We make numerical calculation of oscillator strength for optical transitions between various combinations of electron and hole states, and indeed show oscillator strength of vertically polarized transitions is stronger in our QWR structure. We find that the different effective mass of electrons and holes, especially anisotropic effective mass of holes causes different shapes of wave functions between electrons and holes, which results in larger oscillator strength of vertically polarized transition.

DOI: 10.1103/PhysRevB.68.193304 PACS number(s): 78.67.Lt, 73.21.Hb, 78.66.Fd, 78.45.+h

Polarization properties of one-dimensional (1D) quantum wire (QWR) structures reflect valence-band-mixing of hole states, and demonstrate many interesting aspects peculiar to quasi-1D natures.[1–6] A crescent-shaped QWR structure is formed by growing a quantum well (QW) layer on a patterned substrate with a V groove or a Λ ridge, where thickness variation in a curved QW makes it possible to achieve lateral confinement to realize a QWR. The vertical confinement in the growth direction is stronger than the lateral confinement. Thus, optical anisotropy of a crescent-shaped QWR is expected to be similar to that of a flat QW grown on a planer substrate, where low energy optical transitions are caused by heavy hole (HH) states and are polarized parallel to the QW layer. Recently, however, vertically inclined polarization of lasing[7] and vertically polarized low-energy absorption[6] was observed in V-groove QWRs.

In this paper, we study vertically polarized lasing and spontaneous emissions in a ridge QWR laser. In particular, we find that most of emissions with energies near the band edge are vertically polarized. We make numerical calculation of oscillator strength for optical transitions between various combinations of electron and hole states, and indeed show oscillator strength of vertically polarized transitions is stronger in our QWR structure.

A ridge QWR laser structure is formed via facet growth on a patterned substrate by molecular beam epitaxy (MBE).[8] A cross-sectional transmission electron microscope (TEM) image of a ridge QWR laser structure is shown in Fig. 1. A GaAs layer with a nominal vertical thickness of 5 nm is embedded in 90 nm thick barrier layers of a $Al_{0.2}Ga_{0.8}As$ digital alloy, which provide vertical confinement in the [001] direction. The GaAs layer is slowly curved at the top of the ridge structure, which provides lateral confinement along the GaAs layer. As a result, the QWR is formed at the ridge corner of the two [111]*B* adjacent QWs (side-QWs). A nominal vertical thickness of the GaAs layer in a left-hand region of the structure is slightly thicker than that in a right-hand region. A slight misorientation of atom flux during the MBE growth could cause an asymmetric shape of the potential. The GaAs and $Al_{0.2}Ga_{0.8}As$ layers are sandwiched by the cladding layers of the $Al_{0.4}Ga_{0.6}As$ digital alloy, thus forming an optical waveguide structure. The sample was cleaved to form optical cavities of length $L=300$ μm with the cleaved edges left uncoated. As shown in Fig. 1, we define $\theta=0$ degrees as the growth ([001]) direction, and $\theta=90$ degrees as the $[\bar{1}10]$ direction. The [111]*B* side-QWs are parallel to ± 35.3 degrees from the geometrical crystal orientation.

Polarization dependence of emissions from a cleaved edge of a ridge QWR laser was characterized by optical polarization measurement. Optical excitation was performed by the second harmonics of continuous-wave mode-locked yttrium-lithium fluoride (YLF) laser pulses with the wavelength of 526 nm, the repetition rate of 75.4 MHz, and the pulse duration of 50 ps. The pump laser light was incident on the top of a ridge structure, and was focused via two cylindrical lenses into a stripe region which covered a whole ridge QWR structure uniformly. Carriers are mainly excited at the

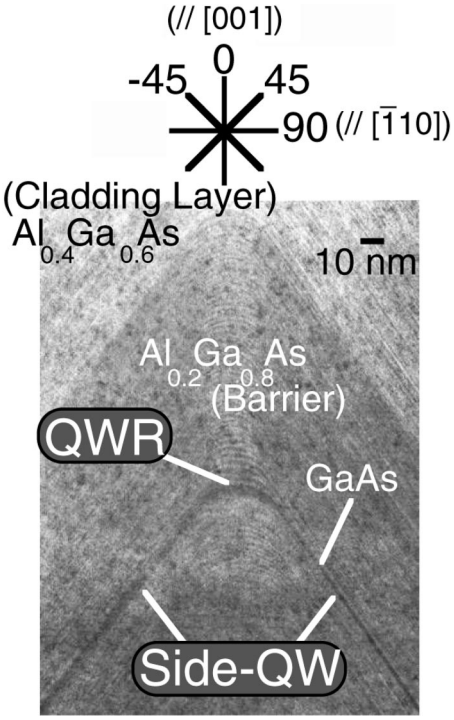

FIG. 1. Cross-sectional transmission electron microscope (TEM) image of a ridge quantum wire (QWR) laser. QWR is formed at the ridge corner of two adjacent QWs (side-QWs). We define $\theta=0°$ as the growth ([001]) direction and $\theta=\pm 90°$ as the $[\bar{1}10]$ direction.

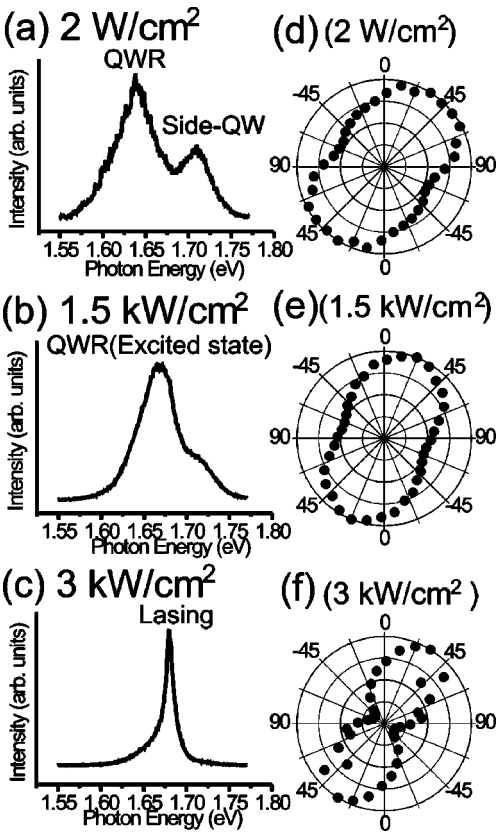

FIG. 2. (a)–(c) PL and lasing spectra of a ridge QWR laser at $T=4.5$ K for excitation powers of (a) 2 W/cm^2, (b) 1.5 kW/cm^2, and (c) 3 kW/cm^2. (d)–(f) Polar plots of polarization at each spectral peak of a QWR in Figs. 2(a)– 2(c) inside a cleaved edge plane. Both PL and lasing are rather vertically polarized. Lasing is linearly polarized.

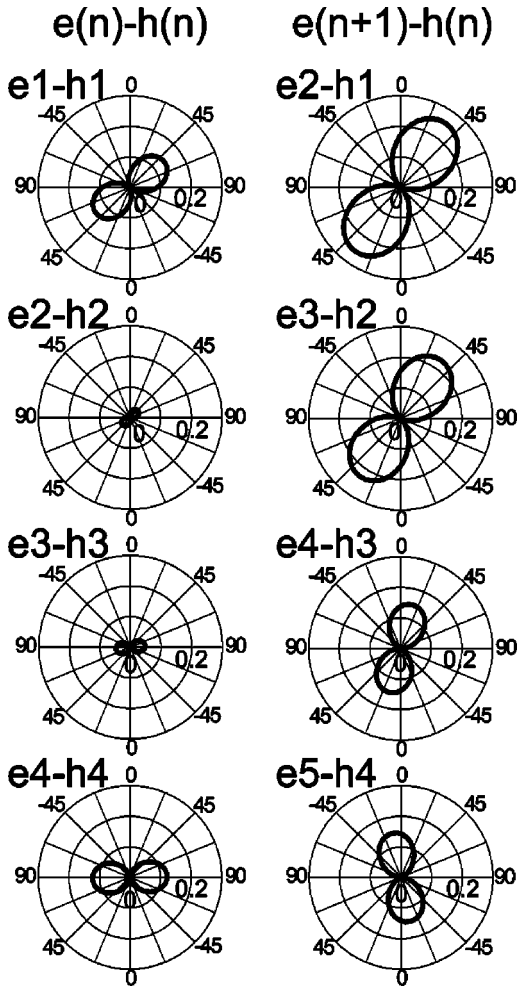

FIG. 3. Calculated results for polarization-dependent oscillator strength for ground- and excited-state transition. The transition of $e1-h1$, $e2-h2$, $e3-h3$, and $e4-h4$ is horizontally polarized and the transition of $e2-h1$, $e3-h2$, $e4-h3$, and $e5-h4$ is vertically polarized. The oscillator strength of vertically polarized transition is larger, which agrees well with the experiments in Fig. 2.

barrier regions of a ridge QWR laser, and flow into the side-QW and QWR regions where they recombine to make spontaneous and stimulated emissions. Emissions from a cleaved edge were collected by an objective lens, passed through a Glan-Thompson polarizer, and were led to a spectrometer.

Figures 2(a)– 2(c) show excitation power dependence of emission spectra at $T=4.5$ K. In Fig. 2(a), emission from the side-QWs and the QWR is observed, whose spectral origins were confirmed by photoluminescence (PL) imaging measurements.[9] As the excitation power is increased in Fig. 2(b), spectral peak showed blueshifts due to state filling, and finally in Fig. 2(c), lasing occurred at interband transition between higher-order excited states.

Figures 2(d)– 2(f) show the polarization dependence of emission intensity at each spectral peak energy of a QWR in (a)–(c). Definition of the polarization angles is shown in Fig. 1. All emissions are rather vertically polarized. For weak excitation power in Fig. 2(d), spontaneous emission from a QWR is polarized to 45°. As we increase the excitation power in Fig. 2(e), the emission becomes to be polarized to 20°. Stimulated emission is linearly polarized to 35° in Fig. 2(f).

We next compute polarization-angle dependent transition matrix elements $|M(\theta)|^2$ for ground- and excited-state transitions, to explain the vertically polarized spontaneous and stimulated emissions. We numerically calculate wave functions of electrons and holes for the potential shown in Fig. 1 based on 4×4 Luttinger Hamiltonian,[10] and compute polarization-angle dependent transition matrix elements. Numerical calculations are done to solve the Schrödinger equations of electrons and holes by finite element method with a $GaAs/Al_{0.2}Ga_{0.8}As$ potential structure extracted from Fig. 1 (see Fig. 4 with a concrete shape of the potential for the calculation). We devide the calculation region into 8720 right triangular elements. Concrete calculation method is written in a separate article.[11]

Figure 3 shows calculated results of square of normalized polarization-angle dependent transition matrix elements $(\hbar/m_0P)^2|M(\theta)|^2$ for ground- and excited-state transitions, where P is the Kane matrix element.[12] Polarization axis of $|M(\theta)|^2$ is nearly horizontal for $e1-h1$, $e2-h2$, $e3-h3$, and $e4-h4$ $[e(n)-h(n)]$ transition, and it is nearly vertical for $e2-h1$, $e3-h2$, $e4-h3$, and $e5-h4$ $[e(n+1)$

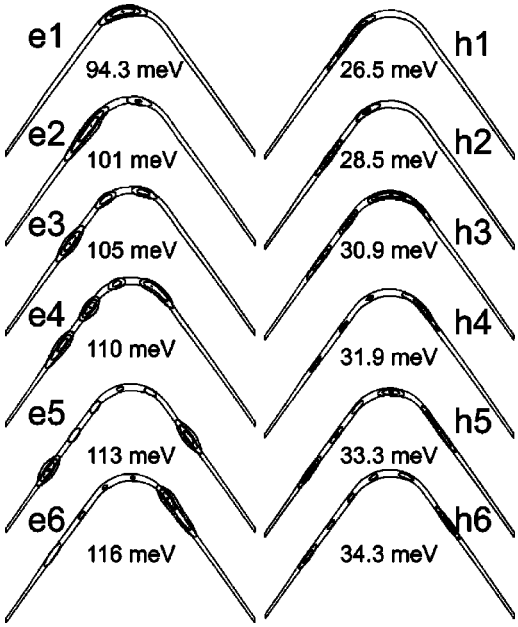

FIG. 4. Contour plots of calculated probability density of electrons ($e1$–$e6$ states) and holes ($h1$–$h6$ states). Quantization energy of each state is also shown. Note that position of maximum probability density of $h(n)$ states is almost the same as that of $e(n+1)$ states due to the different confinement potentials for electrons and holes.

$-h(n)$] transition. The calculated results reveal that oscillator strength of vertically polarized transition [$e(n+1)-h(n)$ transition] is much larger, which well explains our results in Fig. 2.

Next, we explain why the oscillator strength of $e(n+1)-h(n)$ transition is much larger than that of $e(n)-h(n)$ transition in our calculation. Figure 4 shows contour plots of square of wave functions for electrons ($e1,e2,\ldots$) and holes ($h1,h2,\ldots$) obtained by the numerical calculation. Quantization energy of each state is also shown. As quantum number increases, number of nodes in wave functions increases one by one for both electrons and holes. Note that the wave functions of holes largely spread into side-QW regions compared with those of electrons with the same quantum number. This is because effective mass of electrons is light and isotropic, while that of holes is heavy and anisotropic. Effective mass of electrons in GaAs is isotropic and $m_e^* \sim 0.067m_0$ where m_0 is mass of free electrons. On the other hand, effective mass of holes in GaAs is anisotropic, and $m_{h,\perp}^*([001]) \sim 0.34m_0$ toward the [001] direction, and $m_{h,\perp}^*([111]) \sim 0.7m_0$ toward the [111] direction. Thus, there is a relation that

$$m_e^* \ll m_{h,\perp}^*([001]) < m_{h,\perp}^*([111]). \quad (1)$$

Heavier effective mass of holes causes smaller difference of quantization energy between the side-QWs and the QWR. Especially for holes when $m_{h,\perp}^*([111])$ in the side-QW regions is heavier than $m_{h,\perp}^*([001])$ in the QWR region, the difference becomes much smaller. Thus the lateral confinement is much weaker for holes than that for electrons, which makes the wave functions of holes largely spread into the side-QW regions.

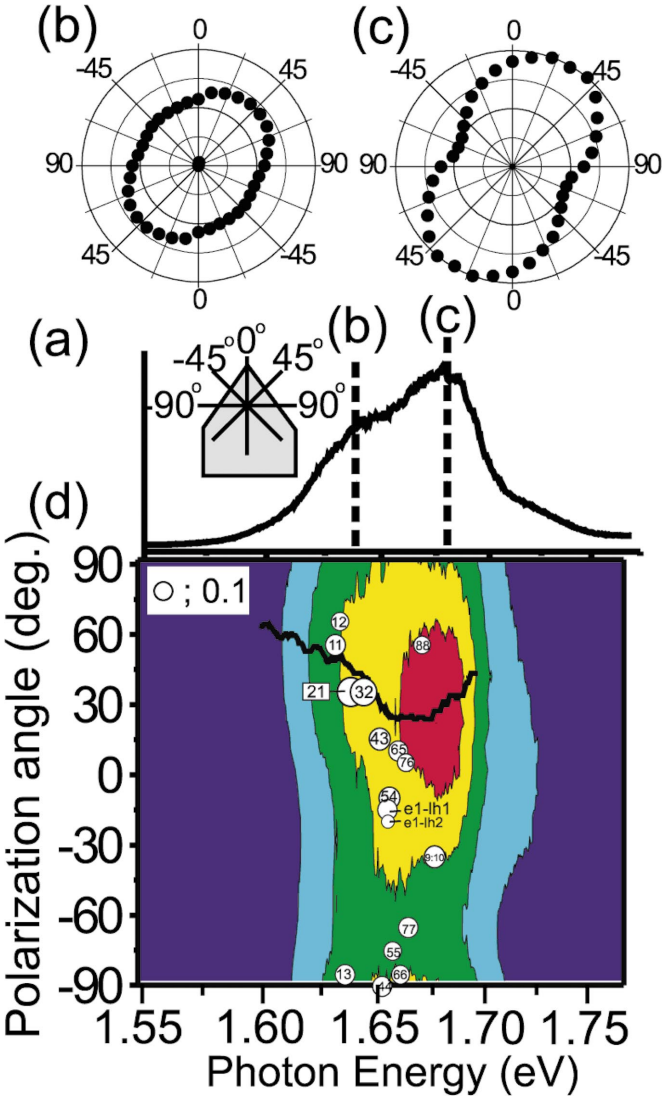

FIG. 5. (Color) (a) PL spectrum with the excitation power of 50 kW/cm^2 at $T=4.5$ K. (b),(c) Polar plots of polarization-dependent PL intensity at (b) ground-state transition energy and (c) lasing photon energy inside a cleaved edge plane. (d) Contour plot of photon-energy and polarization-angle resolved emission intensity of a ridge QWR laser with the excitation power of 50 kW/cm^2 at $T=4.5$ K. A black line shows major polarization axis at each photon energy. Circles show calculation results for ground- and excited-state transitions. Numbers in every circle indicate states of transition (32 means $e3-h2$ transition). Oscillator strength $(\hbar/m_0P)^2|M(\theta)|^2$ is proportional to the area, and the area corresponding to the value of 0.1 is shown in the inset.

Note that positions of maximum probability density of $h(n)$ states are almost the same as those of $e(n+1)$ states due to the different confinement potentials for electrons and holes. Oscillator strength $|M(\theta)|^2$ is determined by overlap integrals of envelope functions of electrons and holes. Larger oscillator strength of e(n+1)-h(n) transition in our calculation is derived from the same positions of maximum probability density of e(n+1) and h(n) states.

We next discuss an effect of an asymmetric potential structure of our sample. The wave functions of holes are much influenced by an asymmetric potential and largely

spreads into left-hand side-QW regions compared with the electron wave functions in Fig. 4. As a result, a position of the maximum probability density of the $h1$ state becomes to be different from that of the $e1$ state, and even the oscillator strength of the ground-state $(e1-h1)$ transition is smaller than that of the $e(n+1)-h(n)$ transition in Fig. 3. Thus asymmetric potential structures also suppress the horizontally polarized $e(n)-h(n)$ transition. In order to achieve a ground state lasing in a ridge QWR, it is important to realize a symmetric potential structure to make the maximum probability density of both e1 and h1 states at the top of the ridge structure.

The transition of $e1-h1$, $e2-h2$, $e2-h1$, and $e3-h2$ is polarized asymmetrically in Fig. 3. This is because the $h1$ and $h2$ states are located at the left-hand QWR region in Fig. 4, and p-orbital Bloch functions of the states is almost parallel to the left-hand side of the potential layer. On the other hand, the transition between the higher order excited states is polarized nearly horizontal $[e(n)-h(n)]$ or vertical $[e(n+1)-h(n)]$ to the potential layer. This is because the wave functions of the higher-order excited states spread into the right-hand QWR region as well, and p-orbital Bloch functions parallel to the right-hand side of the potential also contribute to the polarization property of the transition.

We finally perform point excitation toward a cleaved edge of a ridge QWR laser, to further confirm the correspondence between experimental polarization properties and calculations. An excitation YLF laser is focused to a cleaved edge of the same ridge QWR laser that we achieve lasing in Fig. 2. The excitation power is 50 kW/cm^2 and the temperature is 4.5 K. Figure 5(a) shows spontaneous emission spectrum, and two dotted lines show the ground-state transition energy and the lasing energy. Since we only excite the cleaved edge of the sample, a stimulated emission does not occur and we can measure polarization of spontaneous emission for every transition energy. Figures 5(b) and 5(c) show polar plots of polarization-dependent emission intensity at the ground-state and the lasing photon energy. A spontaneous emission from a QWR is polarized to 45° in Fig. 5(b), and it is polarized to about 30° in Fig. 5(c), which agrees well with the polarization dependence for the uniform excitation in Fig. 2.

A contour plot image in Fig. 5(d) represents photon-energy and polarization-angle resolved emission intensity of the ridge QWR laser with the excitation power of 50 kW/cm^2 at $T=4.5$ K. We measured polarization-dependent emission spectra at every 10° of polarization angle, and arranged them in rows. A black line in Fig. 5(d) shows major polarization axis at each photon energy. The black line shows that major polarization axis of spontaneous emission is 45° at ground state transition energy, and it approaches to be vertical direction until 20° as higher transition energy, and it is 30° at lasing photon energy.

Calculated results of the normalized transition matrix elements for each transition are displayed as many circles in Fig. 5(d). Numbers in every circle indicate quantum numbers of electrons and holes that involve in each interband transition (32 means the $e3-h2$ transition). Oscillator strength is proportional to the area, and we do not display transition with much small oscillator strength. Calculated results show that transition of $e1-h1$ is polarized to 55°. For excited state transition, transition of $e(n+1)-h(n)[e2-h1, e3-h2, e4-h3, \ldots]$ is nearly vertically polarized especially for larger quantum numbers, and their oscillator strength is larger than that of $e1-h1$ transition. These results agree well with the experiment. Transition of $e(n)-h(n)[e4-h4, e5-h5, \ldots]$ is nearly horizontally polarized toward-60° to −90°, but their oscillator strength is much smaller.

The calculated results for transition between electrons and light-hole-like states of holes are also shown in Fig. 5(d) as $e1-lh1$ and $e1-lh2$. These transitions less influence the tendency of polarization properties of a QWR.

In summary, we study vertically polarized lasing and spontaneous emissions in a ridge QWR laser, and theoretically show the mechanism via finite element calculations based on 4×4 Luttinger Hamiltonian. We find that the different effective mass causes different shapes of wave functions between electrons and holes, which results in larger oscillator strength of vertically polarized transition.

This work was partly supported by a Grant-in-Aid from the Ministry of Education, Culture, Sports, Science and Technology, Japan. One of the authors (S.W.) also thanks the Japan Society for the Promotion of Science (JSPS) for partial financial support.

*Present address: Institute of Quantum Electronics and Photonics, Swiss Federal Institute of Technology, 1015 Lausanne, Switzerland. Electronic address: watanabe@dpmail.epfl.ch

†Present address: Advanced Materials Science, Faculty of Engineering, Kagawa University, 2217-20 Hayashi, Takamatsu, Kagawa 761-0396, Japan.

‡Present address: Institute of Industrial Science, University of Tokyo, 4-6-1 Komaba, Meguro-ku, Tokyo 153-8505, Japan.

[1] M. Tsuchiya, J. M. Gaines, R. H. Yan, R. J. Simes, P. O. Holtz, L. A. Coldren, and P. M. Petroff, Phys. Rev. Lett. **62**, 466 (1989).

[2] M. Tanaka and H. Sakaki, Appl. Phys. Lett. **54**, 1326 (1989).

[3] H. Akiyama, T. Someya and H. Sakaki, Phys. Rev. B **53**, R4229 (1996); *ibid.* **53**, R10 520 (1996).

[4] T. Sogawa, H. Ando, S. Ando, and H. Kanbe, Phys. Rev. B **56**, 1958 (1997).

[5] F. Vouilloz, D. Y. Oberli, M.-A. Dupertuis, A. Gustafsson, F. Reinhardt, and E. Kapon, Phys. Rev. Lett. **78**, 1580 (1997); Phys. Rev. B **57**, 12378 (1998).

[6] E. Martinet, M. A. Dupertuis, L. Sirigu, D. Y. Oberli, A. Rudra, K. Leifer, and E. Kapon, Phys. Status Solidi A **178**, 233 (2000).

[7] C. Percival, J. Woodhead, P. A. Houston, A. G. Cuillis, G. Hill, and J. S. Roberts, Appl. Phys. Lett. **77**, 2967 (2000).

[8] S. Koshiba, S. Watanabe Y. Nakamura, M. Yamauchi, M. Yoshita, M. Baba, H. Akiyama, and H. Sakaki, J. Cryst. Growth **201/202**, 810 (1999).

[9] S. Watanabe, S. Koshiba, M. Yoshita, H. Sakaki, M. Baba, and H. Akiyama, Appl. Phys. Lett. **73**, 511 (1998).

[10] J. M. Luttinger and W. Kohn, Phys. Rev. **97**, 869 (1955).

[11] S. Watanabe, M. Yoshita, S. Koshiba, and H. Akiyama, Jpn. J. Appl. Phys. **41**, 5924 (2002).

[12] E. O. Kane, J. Phys. Chem. Solids **1**, 249 (1957).